




# A self-adaptive first-principles approach for magnetic excited states

Zefeng Cai<sup>1</sup>, Ke Wang<sup>1</sup>, Yong Xu<sup>2</sup>, Su-Huai Wei<sup>3</sup> and Ben Xu<sup>4\*</sup> 

## Abstract

The profound impact of excited magnetic states on the intricate interplay between electron and lattice behaviors in magnetic materials is a topic of great interest. Unfortunately, despite the significant strides that have been made in first-principles methods, accurately tracking these phenomena remains a challenging and elusive task. The crux of the challenge that lies before us is centered on the intricate task of characterizing the magnetic configuration of an excited state, utilizing a first-principle approach that is firmly rooted in the ground state of the system. We propose a versatile self-adaptive spin-constrained density functional theory formalism. By iteratively optimizing the constraining field alongside the electron wave function during energy minimization, we are able to obtain an accurate potential energy surface that captures the longitudinal and transverse variations of magnetization in itinerant ferromagnetic Fe. Moreover, this technique allows us to identify the subtle coupling between magnetic moments and other degrees of freedom by tracking energy variation, providing new insights into the intricate interplay between magnetic interactions, electronic band structure, and phonon dispersion curves in single-layered  $\text{CrI}_3$ . This new methodology represents a significant breakthrough in our ability to probe the complex and multifaceted properties of magnetic systems.

Excited magnetic states possess longitudinal and transverse perturbations of magnetic moments that deviate from ground-state magnetic configurations. They are crucial for understanding magnetic ordering, magnetic phase transitions, and other magnetic phenomena. Further, magnetic excited states are prevalent in frustrated magnets [1–4], multiferroics [5–8], superconductors [9–19], topological magnets [20], etc, and are of crucial importance to phenomena such as superconductivity [9–19], quantum critical point [21–24], quantum phase transition [25], and the quantum anomalous Hall effect [26]. The above exotic phenomena stems from the delicate interaction between spin and other degree of freedoms (DoF) such as charge, orbital, and lattice. The elucidation of the microscopic mechanism of these coupling effects need to evaluate the second or higher order derivatives of the energy

with respect to the magnetic moment and other DoFs. In order to do so, the magnetic moment must be considered as a variable that can be altered independently from the other DoFs. And the manifestation of its variation, i.e. the excited magnetic states, is hence critical to understand the mutual interactions, and is significantly challenging to simulate despite its ubiquity.

However, the commonly used density functional theory (DFT) [27] was originally developed to describe ground states. In their seminal works, Dederichs *et al.* [28] and Dudarev *et al.* [29, 30] introduced a Lagrange multiplier  $\lambda$  to constrain the magnetic moments when solving the Kohn-Sham equation as  $\nabla_{\phi_i} L = 0$  [28, 29, 31–34]. However, it is difficult to simultaneously reach the global minimum of Lagrangian and meet the constraint, and thus it is not guaranteed that the magnetic moment  $\mathbf{M}$  gets to its constrained target. This situation is particularly severe in itinerant metallic magnetic materials [35]. Therefore, the magnetic moment is difficult to control and to be considered as a completely independent DoF, and the energy of

\* Correspondence: [bxu@g scaep.ac.cn](mailto:bxu@g scaep.ac.cn)

<sup>4</sup>Graduate School of China Academy of Engineering Physics, Beijing 100088, People's Republic of China

Full list of author information is available at the end of the article

corresponding system is difficult to identify. These uncertainties escalate when the energy is differentiated by an infinitesimal variation of magnetic moment or other DoF, to evaluate the coupling strength, such as the magnetoelectrical coupling constant.

Another unfavorable fact is that these methods require the user to be highly proficient at interactively adjusting the optimization strategy [30, 34], which makes these methods highly prone to numerical error. This is because that the optimization is conducted only in the electronic energy functional minimization, where the constraining parameter  $\lambda$  is set as a pre-defined constant.  $\lambda$ , when improperly chosen, leads the system to a local minimum ( $\lambda$  too small) or to divergence ( $\lambda$  too big). In addition, this fixed  $\lambda$  is difficult to adapt to actual spin fluctuations where different magnetic components exhibit different deviations from the original ground state, which also makes the Hamiltonian numerically unstable to be diagonalized. Recently, Hegde *et al.* [36] developed a self-consistent method to impose spin constraints and sped up the convergence significantly. However, this method only deals with collinear magnetic orders, which hinder the study of complex noncollinear spin fluctuations.

To address these deficiencies, in this letter, we proposed a self-adaptive spin-constrained DFT scheme, where Kohn-Sham orbitals and the constraining vectors are updated iteratively to reach the global optimum of the Lagrangian and the target magnetic moments. In this scheme, the on-site adaptable constraint  $\{\lambda_I\}$  are imposed in the form of a local vector field. The amplitude and orientation of the constraining vector field  $\{\lambda_I\}$  depend on the local magnetic environment of atom  $I$  and vary from component to component. Equipped with this strategy, the magnetic moment can be altered independently from the other DoFs in our non-collinear first-principles scheme. Our approach now paves the way for the investigation of spin fluctuation and its influence on other DoF. To exemplify this method, we then apply it to two scenarios. The first is a spin configuration with confined rotation, using ferromagnetic materials Fe and layered magnetic materials CrI<sub>3</sub> as examples. To simulate real-world fluctuations, it is later generalized to study the electronic band structure of CrI<sub>3</sub> with random magnetic orientations.

## 1 Results

*Self-adaptive spin-constraining algorithm.* Our scheme is sketched in Fig. 1. It is based on the optimization of the Lagrangian function  $L$  under the constraint that the magnetic moment of atom  $I$ , that is,  $\mathbf{M}_I(\{\phi_i\})$ , is the same as the target value denoted by  $\mathbf{M}_I^*$ . To implement this, we design two nested loops updating the Kohn-Sham orbitals  $\{\phi_i\}$  and the Lagrangian multiplier  $\{\lambda_I\}$  respectively.

(i) *Electronic loop:* For a particular  $\lambda_I$ , we can solve

$$\frac{\delta E_{\text{KS}}}{\delta \langle \phi_i |} - \sum_I \lambda_I \cdot \frac{\delta \mathbf{M}_I}{\delta \langle \phi_i |} = \epsilon_i | \phi_i \rangle \quad (1)$$

to obtain a self-consistent solution  $\{\phi_i(\lambda_I)\}$  and the magnetic moment  $\mathbf{M}(\{\phi_i(\lambda_I)\})$ . The atomic magnetic moment  $\mathbf{M}_I$  is generally defined as  $\mathbf{M}_I(\{\phi_i\}) = \text{Tr}(\rho \sigma \hat{\mathcal{V}}_I)$ , where  $\rho$  is the density matrix,  $\sigma$  is the Pauli matrix,  $\hat{\mathcal{V}}_I$  is a pre-defined weight operator for atom  $I$ . Thus, Eq. (1) is obtained as

$$\hat{\mathcal{H}}_{\text{KS}} | \phi_i \rangle - \sum_I \lambda_I \cdot \sigma \hat{\mathcal{V}}_I | \phi_i \rangle = \epsilon_i | \phi_i \rangle. \quad (2)$$

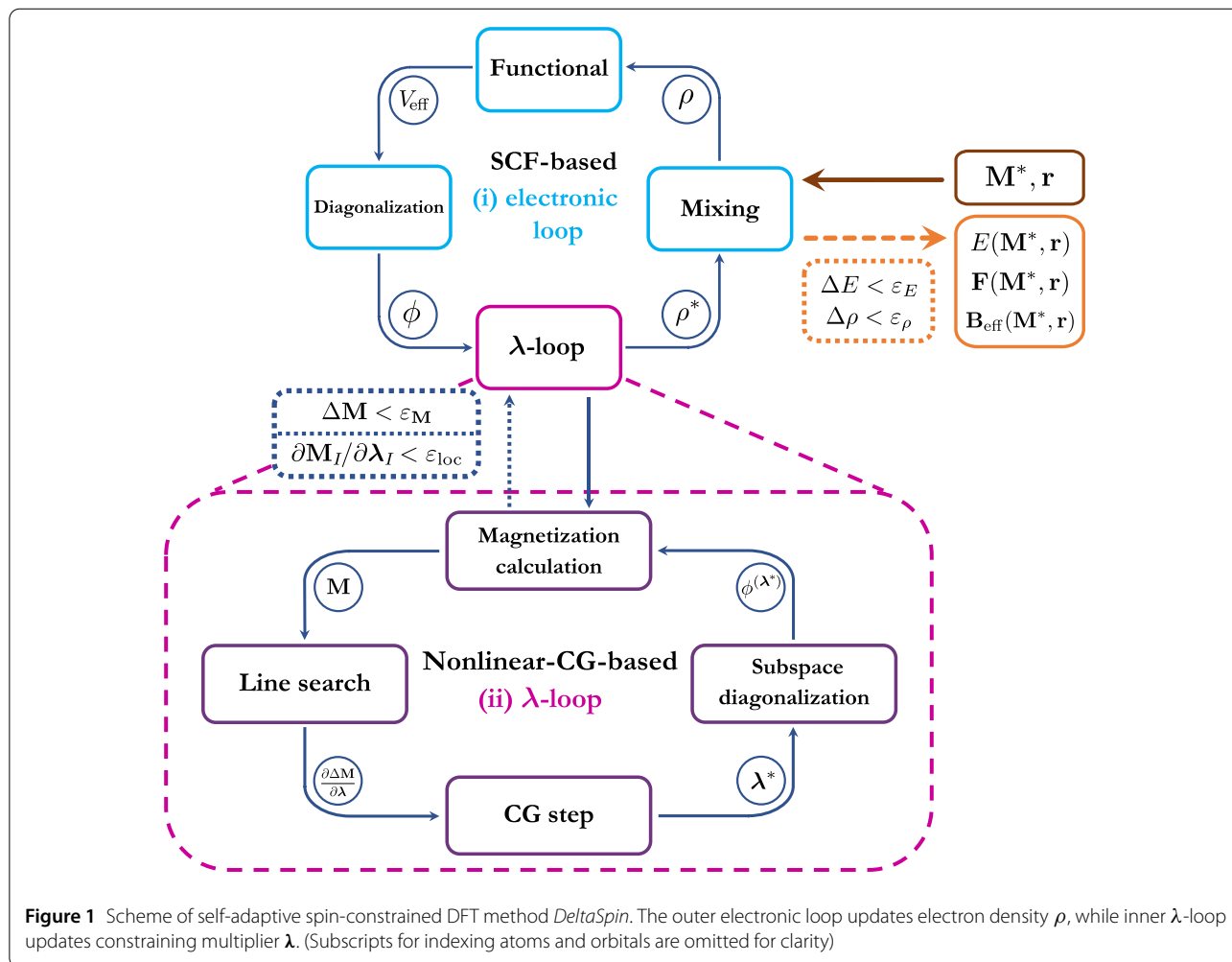
Note that  $\lambda_I$  acts as a constraining field [28].

(ii)  *$\lambda$ -loop:* We can progressively update  $\{\lambda_I\}$  by optimizing

$$\min_{\lambda_I} |\mathbf{M}(\{\phi_i(\lambda_I)\}) - \mathbf{M}^*|^2, \quad (3)$$

that is, the error  $\Delta \mathbf{M}$  between the current magnetization and the target, using the nonlinear conjugate gradient (NCG) method. For an updated  $\lambda_I^*$ , we can solve Eq. (2) via diagonalization in the subspace spanned by the old orbitals  $\{\phi_i(\lambda_I)\}$  to obtain a new set of orbitals  $\{\phi_i(\lambda_I^*)\}$ , and thus, the moment  $\mathbf{M}(\lambda_I^*)$ . In this way, the optimization can continue until a minimum is achieved. A perturbation-like scheme similar to that in Ref. [36] was chosen, which significantly reduced the computational cost compared to diagonalization in the entire basis set. In addition, the  $\lambda$ -loop converged rapidly because the function  $\mathbf{M}(\{\phi_i(\lambda_I)\}) = \partial^2 L / \partial \lambda_I^2$  is proved to be almost monotonous according to the first-order perturbation theory ( $L(\phi_i, \lambda_I, \epsilon_i)$  is a concave function of  $\lambda_I$  at 0 K [33]).

Certain details of the scheme deserve further discussion. In the  $\lambda$ -loop, the gradient of the object function can be approximated as  $2(\mathbf{M}_I - \mathbf{M}_I^*) \frac{\partial \mathbf{M}_I}{\partial \lambda_I}$ , based on the assumption that  $\partial \mathbf{M}_{I' \neq I} / \partial \lambda_I$ , which is the non-local response to the on-site constraining field, is negligible.  $\partial \mathbf{M}_I / \partial \lambda_I$  can be then obtained by lower-complexity estimation strategies for the NCG iteration. To provide better convergence, we control both  $\Delta \mathbf{M} = \sqrt{|\mathbf{M}(\{\phi_i(\lambda_I)\}) - \mathbf{M}^*|^2}$  and the main diagonal of the gradients  $\partial \mathbf{M}_I / \partial \lambda_I$  in the  $\lambda$ -loop. We first introduce a gradually tightened criterion  $\epsilon_M$  for the former, preventing the constraining field from reaching an early stage local minimum. In case of the latter, the loop is programmed to stop when the local response was smaller than an empirical value  $\epsilon_{\text{loc}}$  ( $\epsilon_{\text{loc}} \approx 1 \mu_B^2 / \text{eV}$  works well across our limited tests). This criterion, which is based on the aforementioned localization assumption, is of particular importance. Additionally, the weight operator in Eq. (2) is often an integral in a real-space ball of radius  $r_{\text{cut}}$  with a



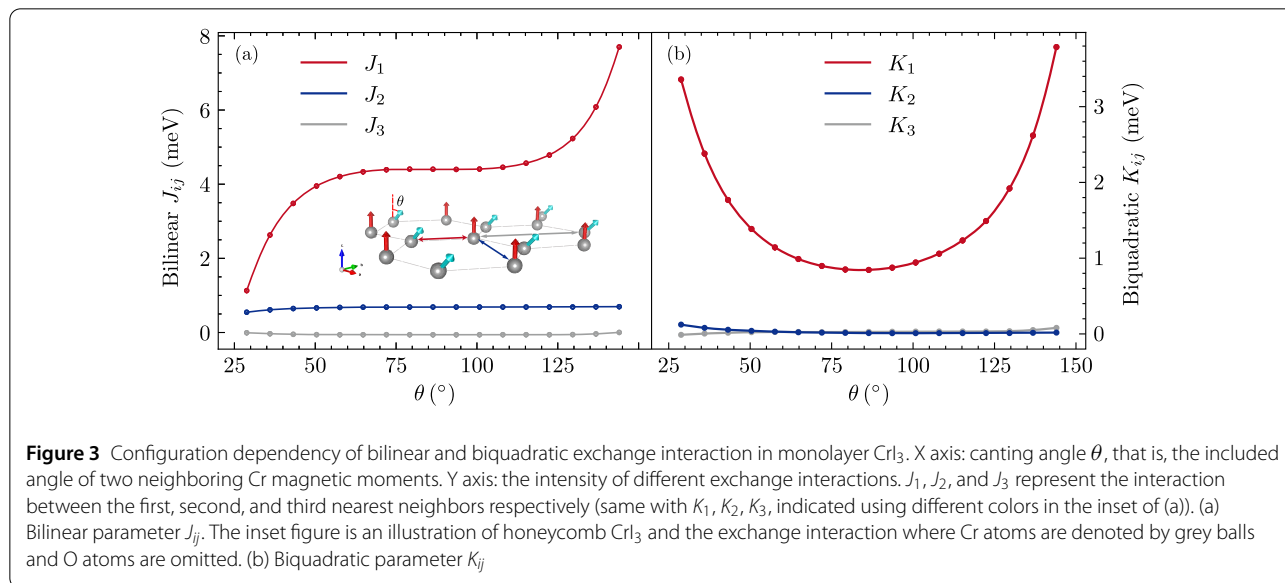
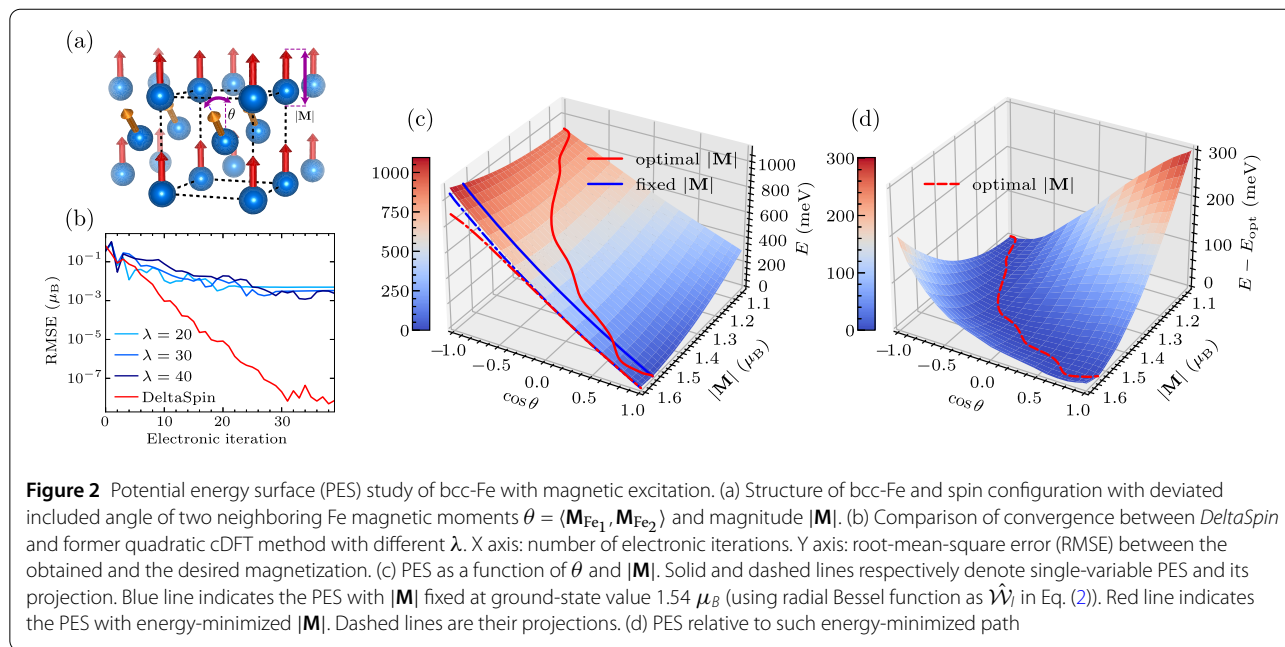
smoothed boundary as  $\hat{W}_I = \int d\mathbf{r} f(r_{\text{cut}} - |\mathbf{r} - \mathbf{r}_I|) |\mathbf{r}\rangle \langle \mathbf{r}|$ . It may take a different form such as the Mulliken partitioning in atomic orbital basis DFT [37].

Upon convergence, the magnetic effective field can be obtained efficiently based on the Hellmann–Feynman theorem as

$$\mathbf{B}_I^{\text{eff}} = -\frac{\delta L(\mathbf{M}_I^*)}{\delta \mathbf{M}_I^*} = -\lambda_I. \quad (4)$$

This suggests that by continuously updating the constraining field,  $\Delta \mathbf{M}$  is minimized and an increasingly accurate estimation of the magnetic effective field is obtained, which turns out to be the constraining field  $\lambda_I$  itself. This estimation shows good correspondence with the true value, which is obtained via differentiation near the collinear limit, and a relative error of up to 4% through the entire path of non-collinear rotation (see Fig. S2 in the Additional file 1). This is because Eq. (4) is strictly correct only if  $\langle \phi_i | \nabla_{\mathbf{M}_I} \hat{H}_{\text{KS}} | \phi_i \rangle$  is negligible [38].

**Potential energy surface.** A fine-grid potential energy surface (PES) is of great significance, particularly the one considering the spin DoF. While the previous quadratic cDFT requires a predetermined multiplier  $\lambda$  and may collapse during the early stage of the electronic loop (an analysis is presented in the Additional file 1), the proposed method can self-adaptively update the multiplier and exhibits a much better precision and efficiency. We studied the magnetic PES of the bcc-Fe (Fig. 2). The two DoFs scanned were the magnitude of atomic moments  $|\mathbf{M}|$  and the included angle between the nearest neighbors' moments  $\theta$ . In the calculations using former quadratic constraints, the root-mean-square error (RMSE) between the obtained and desired spin configurations were stuck at approximately  $10^{-2} \mu_B$  (blue lines in Fig. 2(b)). In comparison, the *DeltaSpin* algorithm exhibited a much better convergence, where the RMSE decreased rapidly to nearly zero ( $10^{-8} \mu_B$ ) for the same number of electronic iterations. We found that the energy-favored magnitude increased when the spins approached the ferromagnetic (FM) order and decreased when approaching anti-ferromagnetic (AFM)



order. Moreover, the magnitude-optimized energy curve was the PES calculated using the former direction-only constraining method, which is a subset of our  $V(|\mathbf{M}|, \theta)$  PES.

**Effects on magnetic interactions.** One of the advantages of this method is the ability to obtain the real on-site magnetic interaction around an arbitrary magnetic configuration through simple calculations of the first derivative of energy  $E$  with respect to  $\mathbf{M}$ . This was not possible in previous studies as achieving precision for both  $E$  and  $\delta\mathbf{M}$  was challenging. In Fig. 3, we show the calculated  $J_{ij}$  and  $K_{ij}$  as the bilinear exchange and biquadratic exchange pa-

rameters with variation in the magnetic configurations. The effective Hamiltonian used was  $H = -\sum_{i,j>i} J_{ij}(\mathbf{e}_i \cdot \mathbf{e}_j) - \sum_{i,j>i} K_{ij}(\mathbf{e}_i \cdot \mathbf{e}_j)^2$ , where  $i, j$  is the atom index. Both  $J_1$  and  $K_1$  exhibited strong dependency on the local magnetic configurations, as shown in Fig. 3. Further,  $J_1$  from the previous energy-mapping strategy, which is a constant at approximately 3 meV [39], was between the maximum and the minimum of the result obtained.

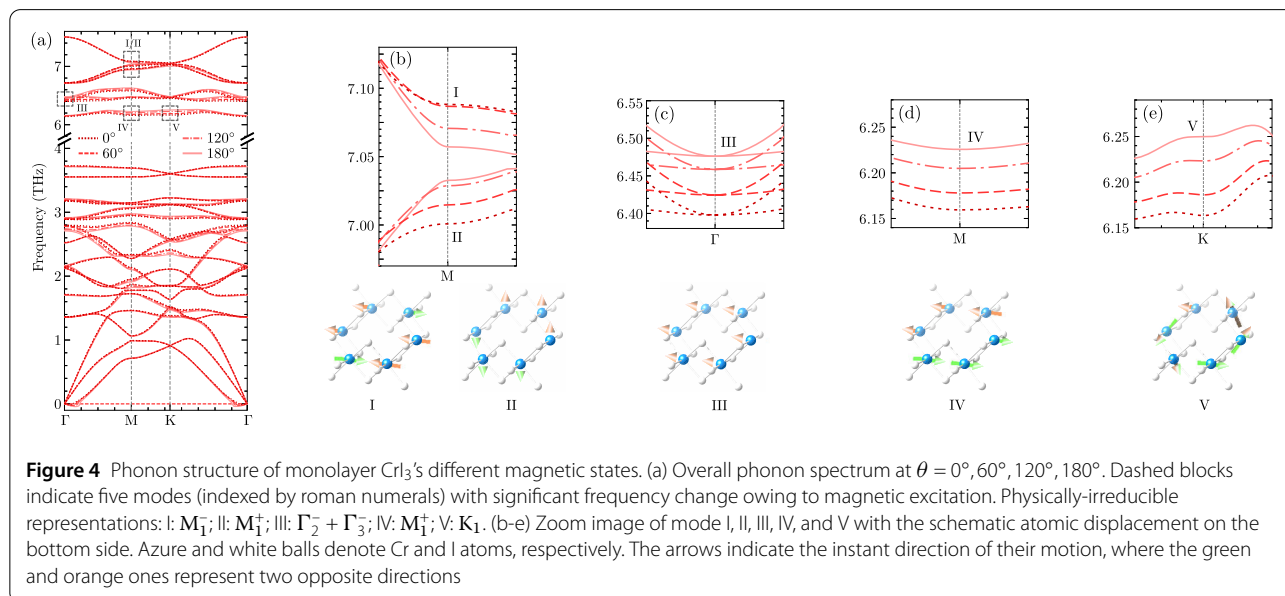
The magnetic effective fields  $\frac{\delta E}{\delta \mathbf{M}}$  and magnetic torques  $\frac{\delta E}{\delta \mathbf{e}}$  are generally considered as the indicators of magnetic interactions and could be employed as the driving forces in further dynamical simulations using real-time TDDFT

or the Landau-Lifshitz-Gilbert(Bloch) method. There are two different strategies to calculate them: (i) Finite difference approximation directly using the definition, that is, taking derivatives of the total energy  $E$  with respect to  $\mathbf{M}_i^z$ ; (ii) Hellmann–Feynman approximation, that is, the constraining field, explained above.

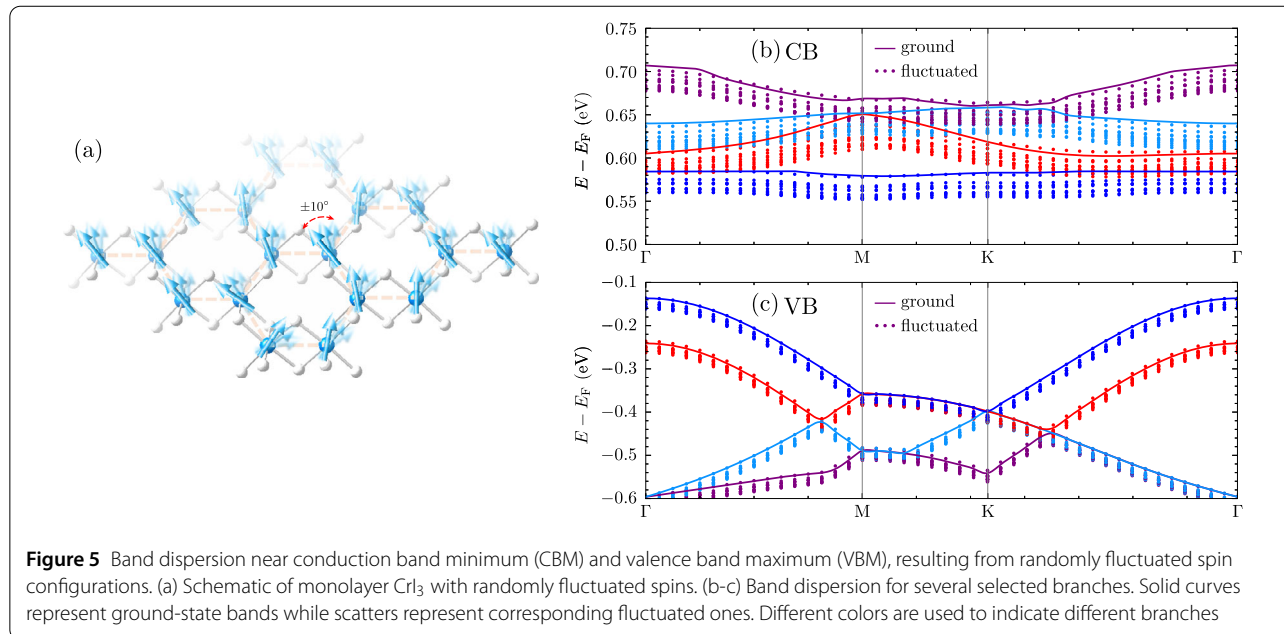
We calculated such constraining-field-approximated magnetic torques and compared them to the finite-differentiated ones in bcc-Fe and monolayer  $\text{CrI}_3$  (see Fig. S2). The maximum relative error was about 4%, which was attributed to the non-collinear contribution in Kohn-Sham functional  $\langle \phi_i | \nabla_{\mathbf{M}_i} \hat{\mathcal{H}}_{\text{KS}} | \phi_i \rangle$ , and perfectly acceptable in some cases. Notice that the difference was negligible in the collinear limit, that is, in the neighborhood of FM and AFM order, both in Fe and in  $\text{CrI}_3$ . It means that Hellmann–Feynman approximation is a efficient and reliable choice given that the complexity of explicit differentiation is at least  $\mathcal{O}(N)$  ( $N$  is the number of atoms) whereas to obtain constraining field only one calculation is needed. In addition, if a delicate description instead of a crude estimate of magnetic dynamics is needed, one can always apply an infinitesimal change to spin moments, recalculate the total energy, and take the derivatives. This procedure is also unachievable for  $\lambda$ -fixed constraining formalism wherein the inadequate precision of energy leads to poor precision of magnetic torques.

**Effects on lattice dynamics.** The variation in spin configuration has a non-trivial influence on phonon behaviors, and this study proposed a straightforward method to identify such couplings. This was performed by combining the frozen phonon method [40] with *DeltaSpin*. In particular, the system’s energy must be precisely calculated at the atomic and magnetic excitations. Simultaneously, the magnetic configuration must be prevented from

“drifting away”. *DeltaSpin* can limit the energy and on-site moment error to  $10^{-9}$  eV and  $10^{-7} \mu_B$ , respectively, while maintaining efficiency with more than one hundred atoms; to the best of our knowledge, it is the only method that can access this type of phonon calculations. Four selected spin-fluctuating states were obtained for  $\text{CrI}_3$  (Fig. 4). Only the moments of chromium were constrained, while iodine atoms were fully relaxed, owing to the functionality of *DeltaSpin* to selectively constrain atoms or components. We found five modes that were significantly influenced by magnetic excitation, all of which appeared in the high-frequency branches where the Cr vibrations dominated (Fig. 4(a)). Regardless of spin-orbit coupling and anti-symmetric exchange, these frequency shifts can be roughly explained by the change in the “Heisenberg-only” force constant.  $[\partial J_{ij} / \partial \mathbf{r}] [\mathbf{e}_i \cdot \mathbf{e}_j]$ . The second term depends on the spin configuration explicitly. The first term, which is mainly contributed by the competition between the AFM  $t_{2g}$ - $t_{2g}$  and FM  $t_{2g}$ - $e_g$  interactions [41], also experiences considerable changes because of the different occupancies of  $e_g$  and  $t_{2g}$  orbitals across all four configurations. The existence of “collective-motion” modes, in which the distance between any two Cr atoms remains unchanged (Fig. 4(c),  $\Gamma_2^- + \Gamma_3^-$ ), indicates that the interaction between Cr and I atoms, that is, the metal-ligand interaction, is also strongly affected by only changing the on-site moments of metal atoms. Moreover, the moments of I relax from  $10^{-1} \mu_B$  to approximately zero as  $\theta$  increases from  $0^\circ$  to  $180^\circ$ , whose importance has been demonstrated by previous research [42–45]. Using this algorithm, we can obtain the spin-lattice interaction information. Consequently, the process starts from the objective of obtaining a particular magnetic configuration to determine a feasible method



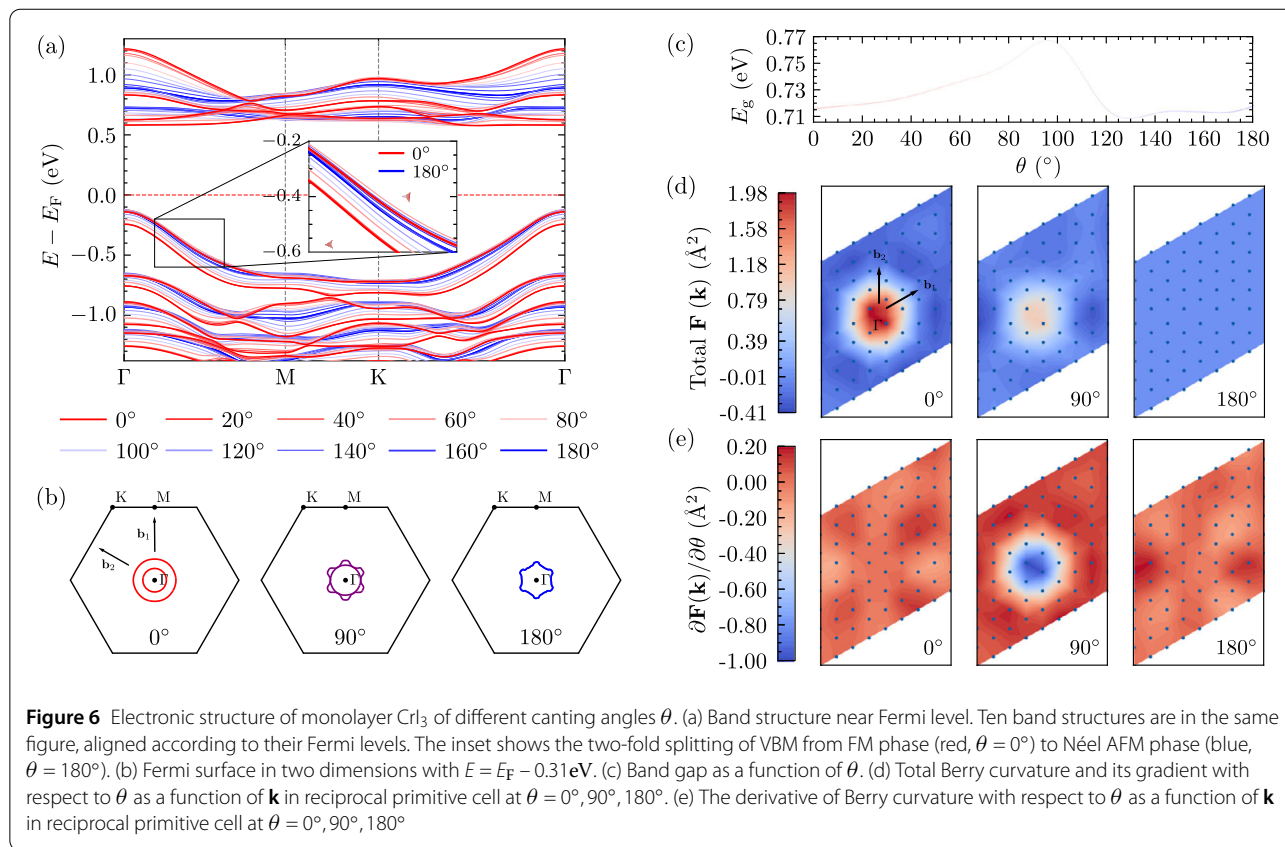




of selective excitation via lattice vibrations. Thus, this can guide ultrafast THz experiments through resonant excitation of infrared (IR) [46] or Raman-active phonons [47].

**Effects on electronic structure.** Spin fluctuations have a prominent effect on the electronic structure such as the band structure and orbital character of the Fermi surface [48–50]. First-principles calculations of electronic structures with spin fluctuations are a critical input for further evaluating the many-body effect [51]. Here, we demonstrate that the band structure is profoundly affected by spin fluctuations using the constrained method (Fig. 5). We modeled several spin-fluctuating configurations near the ground state of monolayer  $\text{CrI}_3$ , wherein magnetic moments were drawn at random from the uniform distribution within the FM order  $\pm 10^\circ$ . Their “excited” Kohn-Sham orbitals were then precisely calculated following the DFT routine, which distinguished our method from TDDFT utilizing the expansion of the ground state. Different branches from the obtained bands showed slightly different broadening behaviors with amplitudes varying in the range of 30–50 meV; consequently, the bandgap shifted. In addition, we obtained several electronic states with different canting angles  $\theta$  in the transition from the FM to the Néel AFM phase of  $\text{CrI}_3$ . These exhibited prominent variation in the band gap, Fermi surface, and topological features (see Fig. S4–5 in the Additional file 1). Thus, this method can be a potentially useful strategy to access a spin-renormalized band structure that fully considers the coupling between spin and electronic DoF [11], which is exceptionally useful for investigating fundamental low-energy physics or exploring rich functionalities in dynamic or optical properties.

The wave function is solved precisely via DeltaSpin for spin-fluctuating states. Thus, we are able to depict more detailed electronic structure. Strong interplay between magnetism and topology of electronic states was found, bringing forth rich functionalities in dynamical or optical properties. The topological sensibility to the magnetic configuration was observed for the first time using cDFT. We modeled ten excited states with different canting angles  $\theta$  in the transition from FM to Néel AFM phase of monolayer  $\text{CrI}_3$ . They exhibited significant variation in band structure, band gap, and Fermi surface as shown in Fig. 6. We noticed the splitting of every two-fold degenerate band when  $\theta$  went from  $180^\circ$  to  $0^\circ$ , following the parity-time (PT) symmetry breaking from AFM to FM phase. It could be further demonstrated in Fermi surface, where one hexagon-shape band in AFM phase split into two concentric circle-shaped valence bands in FM phase (Fig. 6(b)). This process happened on  $\Gamma$ -M path first, then on  $\Gamma$ -K. Simultaneously, the band gap went through a variation of about 50 meV. Moreover, we demonstrated the change in Berry curvature  $\mathbf{F}(\mathbf{k})$  and its sensitivity  $\partial\mathbf{F}(\mathbf{k})/\partial\theta$  throughout the process (see Fig. 6(d–e)), These were calculated using Fukui’s formalism, defined as  $\mathbf{F}(\mathbf{k}) \equiv \ln[U_1(\mathbf{k})U_2(\mathbf{k}+\hat{1})U_1(\mathbf{k}+\hat{2})^{-1}U_2(\mathbf{k})^{-1}]$ , where  $\hat{1}(\hat{2})$  denotes the reciprocal basis vector and  $U_{1(2)}$  represents a purposely defined U(1) link variable [52]. However, the Chern number [53], obtained by integrating the Berry curvature over the Brillouin zone, shows no dependence on the magnetic configuration because  $\text{CrI}_3$  is, as a whole, a trivial insulator.



## 2 Discussion

This study proposes a self-adaptive spin-constrained DFT method wherein the spin fluctuations or magnetic excitation were incorporated along with spin-orbit coupling and non-collinear magnetic configurations, capable of dealing with full degrees of freedom of the amplitude and rotation angle from both magnetic and ligand atoms [45]. This enabled us to gain further insight into spin fluctuations from the electron, lattice, and magnetic perspectives, and also get access to the wave function of magnetic excited states. Here we demonstrate the broadening of band because of the random perturbations of magnetic moments, while this can be easily scaled to different temperature and the broadening with  $k$  dependence can be an indicator to real coupling between spin and other DoFs such as electron and lattice. In addition, the obtained precise atomic forces and magnetic effective fields could be employed as the driving forces in further dynamical simulations such as Landau–Lifshitz–Gilbert (or Landau–Lifshitz–Bloch) or TDDFT [54, 55]. Moreover, the rapid calculation of energy and its corresponding derivatives indicate its ability as a systematic data generator for machine learning surrogate models [56–60] and is expected to be revolutionary with its ability to obtain arbitrary spin-lattice configurations with first-principles precision and high efficiency.

## 3 Methods

**Spin-constrained approach.** The spin-constrained DFT calculations have been performed using the self-adaptive spin-constraining algorithm *DeltaSpin*, which has been implemented as a loadable module for Vienna Ab initio Simulation Package (VASP) [61–63]. The tolerance  $\epsilon_M$  for all the constrained local magnetic moments was  $10^{-8} \mu_B$ . In Fe bulk, the magnetic moments of all Fe atoms were constrained to required values. In  $\text{CrI}_3$ , only the magnetic moments of Cr atoms were constrained and those of I atoms were set to be fully relaxed. For the finite difference calculations of magnetic effective fields, a  $10^{-3}$  rad interval was used to approximate an infinitesimal variation when calculating  $\Delta E / \Delta \mathbf{e}$ .

**Density functional theory calculations.** All the structural optimization and electronic structure calculations have been performed with VASP at the level of density functional theory with the Perdew–Burke–Ernzerhof (PBE) functional. The energy cut off was 600 eV for the plane-wave basis of the valence electrons in bulk Fe and 520 eV for monolayer  $\text{CrI}_3$ . The DFT + U approach with  $U = 5.3$  eV is applied for Cr in  $\text{CrI}_3$ . Total energy tolerance for electronic structure minimization was  $10^{-8}$  eV and a  $\Gamma$ -centered mesh with  $k$ -spacing  $0.06\pi \text{ \AA}^{-1}$  was applied for both two systems. The VASPBERRY code [64] was used to calculate Berry curvature and Chern number directly from

the output of VASP. For the phonon calculations, Phonopy was used to create a  $3 \times 3 \times 1$  supercell structure for monolayer  $\text{CrI}_3$  and VASP was then employed to calculate the force constants.

**Local mapping of the spin Hamiltonian.** Inspired by the energy-mapping method [65], we defined “canting angle”  $\theta$  in honeycomb-like  $\text{MX}_3$  as Fig. S3. We fit a “local” second-order polynomial around  $\theta^*$  to the total energy of certain configurations with different  $\theta$  as follows:

$$H = - \sum_{i<j} J_{ij}(\hat{\mathbf{e}}_i \cdot \hat{\mathbf{e}}_j) - \sum_{i<j} K_{ij}(\hat{\mathbf{e}}_i \cdot \hat{\mathbf{e}}_j)^2 \quad (5)$$

$$= a_0(\theta^*) + a_1(\theta^*) \cdot \cos \theta + a_2(\theta^*) \cdot \cos^2 \theta, \quad (6)$$

where  $\theta$  is in the neighborhood of  $\theta^*$ , that is,  $\theta \in (\theta^* - \delta\theta, \theta^* + \delta\theta)$ . Notice that all coefficients of the polynomial implicitly depends on the centered  $\theta^*$ . After deduction,  $\theta^*$ -centered pair-wise exchange parameters from the first nearest neighbor (1-NN) up to 3-NN can be solved via

$$\begin{pmatrix} 6 & 0 & 6 \\ 2 & 8 & 6 \\ 4 & 8 & 0 \end{pmatrix} \begin{pmatrix} J_1, K_1 \\ J_2, K_2 \\ J_3, K_3 \end{pmatrix} = - \begin{pmatrix} a_1^N, a_2^N \\ a_1^Z, a_2^Z \\ a_1^S, a_2^S \end{pmatrix}, \quad (7)$$

where the dependency of all quantities on  $\theta^*$  are omitted. N for Néel, Z for Zigzag, S for Stripy. These exchange parameters can be treated as the local exchange parameters at  $\theta^*$ .

## Supplementary information

**Supplementary information** accompanies this paper at <https://doi.org/10.1007/s44214-023-00041-1>.

**Additional file 1.** See Supplementary Material for discussions on previous Lagrangian-based constraining method, calculations of spin spirals, and more details about exchange parameter fitting. (PDF 1.0 MB)

## Acknowledgements

We appreciate Han Wang, Kun Cao, C. Freysoldt for their helpful discussions.

## Funding

Open access funding provided by Shanghai Jiao Tong University. This work was funded by the National Natural Science Foundation of China (Grant Nos. U2330401 and 51790494).

## Availability of data and materials

All the relevant data discussed in the present paper are available from the authors on request. Spin-constrained calculations were conducted with the *DeltaSpin* code (<https://github.com/caizefeng/DeltaSpin>).

## Declarations

### Ethics approval and consent to participate

Not Applicable.

### Consent for publication

Not Applicable.

## Competing interests

YX is an editorial board member for *Quantum Frontiers* and was not involved in the editorial review, or the decision to publish, this article. All authors declare that there are no competing interests.

## Author contributions

BX conceived and instructed the research. Under the guidance of BX, ZC performed the theoretical derivation, code implementation, and data analysis. KW, YX, and SW contributed to the interpretation of the results. ZC and BX wrote the manuscript with the input from KW, YX, and SW. All authors read and approved the final manuscript.

## Author details

<sup>1</sup>School of Materials Science and Engineering, Tsinghua University, Beijing 100084, People's Republic of China. <sup>2</sup>Department of Physics, Tsinghua University, Beijing 100084, People's Republic of China. <sup>3</sup>Beijing Computational Science Research Center, Beijing 100193, People's Republic of China. <sup>4</sup>Graduate School of China Academy of Engineering Physics, Beijing 100088, People's Republic of China.

Received: 24 October 2023 Revised: 8 November 2023

Accepted: 13 November 2023 Published online: 04 December 2023

## References

- Lee S-H, Broholm C, Ratcliff W, Gasparovic G, Huang Q, Kim TH, Cheong S-W (2002) Emergent excitations in a geometrically frustrated magnet. *Nature* 418:856
- Pelissetto A, Vicari E (2002) Critical phenomena and renormalization-group theory. *Phys Rep* 368:549
- Balents L (2010) Spin liquids in frustrated magnets. *Nature* 464:199
- Nisoli C, Moessner R, Schiffer P (2013) Colloquium: artificial spin ice: designing and imaging magnetic frustration. *Rev Mod Phys* 85:1473
- Tokura Y, Seki S, Nagaosa N (2014) Multiferroics of spin origin. *Rep Prog Phys* 77:076501
- Xiang HJ, Wei S-H, Whangbo M-H, Da Silva JLF (2008) Spin-orbit coupling and ion displacements in multiferroic  $\text{TbMnO}_3$ . *Phys Rev Lett* 101:037209
- Fabrèges X, Petit S, Mirebeau I, Pailhès S, Pinsard L, Forget A, Fernandez-Diaz MT, Porcher F (2009) Spin-lattice coupling, frustration, and magnetic order in multiferroic  $\text{RMnO}_3$ . *Phys Rev Lett* 103:067204
- Lee S, Pirogov A, Han JH, Park J-G, Hoshikawa A, Kamiyama T (2005) Direct observation of a coupling between spin, lattice and electric dipole moment in multiferroic  $\text{ymno}_3$ . *Phys Rev B* 71:180413
- Anderson PW (1984) Heavy-electron superconductors, spin fluctuations, and triplet pairing. *Phys Rev B* 30:1549
- Sidis Y, Braden M, Bourges P, Hennion B, NishiZaki S, Maeno Y, Mori Y (1999) Evidence for incommensurate spin fluctuations in  $\text{Sr}_2\text{RuO}_4$ . *Phys Rev Lett* 83:3320
- Kuwabara T, Ogata M (2000) Spin-triplet superconductivity due to antiferromagnetic spin-fluctuation in  $\text{Sr}_2\text{RuO}_4$ . *Phys Rev Lett* 85:4586
- Mazin II, Singh DJ (1997) Ferromagnetic spin fluctuation induced superconductivity in  $\text{Sr}_2\text{RuO}_4$ . *Phys Rev Lett* 79:733
- Tranquada JM, Buyers WJL, Chou H, Mason TE, Sato M, Shamoto S, Shirane G (1990) Spin fluctuations in superconducting  $\text{YBa}_2\text{Cu}_3\text{O}_{6.5}$ . *Phys Rev Lett* 64:800
- Monthoux P, Pines D (1992) Spin-fluctuation-induced superconductivity in the copper oxides: a strong coupling calculation. *Phys Rev Lett* 69:961
- Mook HA, Dai P, Hayden SM, Aeppli G, Perring TG, Doğan F (1998) Spin fluctuations in  $\text{YBa}_2\text{Cu}_3\text{O}_{6.6}$ . *Nature* 395:580
- Lumsden MD, Christianson AD, Goremychkin EA, Nagler SE, Mook HA, Stone MB, Abernathy DL, Guidi T, MacDougall GJ, de la Cruz C, Sefat AS, McGuire MA, Sales BC, Mandrus D (2010) Evolution of spin excitations into the superconducting state in  $\text{FeTe}_{1-x}\text{Se}_x$ . *Nat Phys* 6:182
- Chen T, Chen Y, Kreisler A, Lu X, Schneidewind A, Qiu Y, Park JT, Perring TG, Stewart JR, Cao H, Zhang R, Li Y, Rong Y, Wei Y, Andersen BM, Hirschfeld PJ, Broholm C, Dai P (2019) Anisotropic spin fluctuations in detwinned  $\text{FeSe}$ . *Nat Mater* 18:709
- Moriya T, Ueda K (2000) Spin fluctuations and high temperature superconductivity. *Adv Phys* 49:555
- Moriya T, Ueda K (2003) Antiferromagnetic spin fluctuation and superconductivity. *Rep Prog Phys* 66:1299
- Li J, Li Y, Du S, Wang Z, Gu B-L, Zhang S-C, He K, Duan W, Xu Y (2019) Intrinsic magnetic topological insulators in van der Waals layered  $\text{MnBi}_2\text{Te}_4$ -family materials. *Sci Adv* 5:eaaw5685



21. Rosch A (1999) Interplay of disorder and spin fluctuations in the resistivity near a quantum critical point. *Phys Rev Lett* 82:4280
22. Georges A, Parcollet O, Sachdev S (2001) Quantum fluctuations of a nearly critical Heisenberg spin glass. *Phys Rev B* 63:134406
23. Ishida K, Okamoto K, Kawasaki Y, Kitaoka Y, Trovarelli O, Geibel C, Steglich F (2002)  $\text{YbRh}_2\text{Si}_2$ : spin fluctuations in the vicinity of a quantum critical point at low magnetic field. *Phys Rev Lett* 89:107202
24. v. Löhnneysen H, Rosch A, Vojta M, Wölfle P (2007) Fermi-liquid instabilities at magnetic quantum phase transitions. *Rev Mod Phys* 79:1015
25. Zhang J, Chang C-Z, Tang P, Zhang Z, Feng X, Li K, Wang LL, Chen X, Liu C, Duan W, He K, Xue Q-K, Ma X, Wang Y (2013) Topology-driven magnetic quantum phase transition in topological insulators. *Science* 339:1582
26. Li Y-H, Cheng R (2021) Spin fluctuations in quantized transport of magnetic topological insulators. *Phys Rev Lett* 126:026601
27. Kohn W, Sham LJ (1965) Self-consistent equations including exchange and correlation effects. *Phys Rev* 140:A1133
28. Dederichs PH, Blügel S, Zeller R, Akai H (1984) Ground states of constrained systems: application to cerium impurities. *Phys Rev Lett* 53:2512
29. Ma P-W, Dudarev SL (2015) Constrained density functional for noncollinear magnetism. *Phys Rev B* 91:054420
30. Dudarev SL, Liu P, Andersson DA, Stanek CR, Ozaki T, Franchini C (2019) Parametrization of **LSDA + U** for noncollinear magnetic configurations: multipolar magnetism in  $\text{UO}_2$ . *Phys Rev Mater* 3:083802
31. Richter M, Nitzsche U, Eschrig H (1995) Constrained density functional calculations for magnetic systems. *J Magn Magn Mater* 140–144:207. International Conference on Magnetism
32. Stocks GM, Ujfalussy B, Wang X, Nicholson DMC, Shelton WA, Wang Y, Canning A, Györfly BL (1998) Towards a constrained local moment model for first principles spin dynamics. *Philos Mag B* 78:665
33. Wu Q, Van Voorhis T (2005) Direct optimization method to study constrained systems within density-functional theory. *Phys Rev A* 72:024502
34. Kurz P, Förster F, Nordström L, Bihlmayer G, Blügel S (2004) Ab initio treatment of noncollinear magnets with the full-potential linearized augmented plane wave method. *Phys Rev B* 69:024415
35. Zimmermann B, Bihlmayer G, Böttcher M, Bouhassoune M, Lounis S, Sinova J, Heinze S, Blügel S, Dupé B (2019) Comparison of first-principles methods to extract magnetic parameters in ultrathin films:  $\text{Co/Pt}(111)$ . *Phys Rev B* 99:214426
36. Hegde O, Grabowski M, Zhang X, Waseda O, Hickel T, Freysoldt C, Neugebauer J (2020) Atomic relaxation around defects in magnetically disordered materials computed by atomic spin constraints within an efficient Lagrange formalism. *Phys Rev B* 102:144101
37. Cuadrado R, Pruneda M, García A, Ordejón P (2018) Implementation of non-collinear spin-constrained **DFT** calculations in siesta with a fully relativistic Hamiltonian. *J Phys, Mater* 1:015010
38. Streib S, Borisov V, Pereiro M, Bergman A, Sjöqvist E, Delin A, Eriksson O, Thonig D (2020) Equation of motion and the constraining field in ab initio spin dynamics. *Phys Rev B* 102:214407
39. Ke L, Katsnelson MI (2021) Electron correlation effects on exchange interactions and spin excitations in 2d van der Waals materials. *npj Comput Mater* 7:1
40. Togo A, Tanaka I (2015) First principles phonon calculations in materials science. *Scr Mater* 108:1
41. Sadhukhan B, Bergman A, Kvashnin YO, Hellsvik J, Delin A (2022) Spin-lattice couplings in two-dimensional  $\text{CrI}_3$  from first-principles computations. *Phys Rev B* 105:104418
42. Ye M, Vanderbilt D (2014) Dynamical magnetic charges and linear magnetoelectricity. *Phys Rev B* 89:064301
43. Ye M, Vanderbilt D (2015) Magnetic charges and magnetoelectricity in hexagonal rare-earth manganites and ferrites. *Phys Rev B* 92:035107
44. Logemann R, Rudenko AN, Katsnelson MI, Kirilyuk A (2017) Exchange interactions in transition metal oxides: the role of oxygen spin polarization. *J Phys Condens Matter* 29:335801
45. Solov'yev IV (2021) Exchange interactions and magnetic force theorem. *Phys Rev B* 103:104428
46. Foteinopoulou S, Devarapu GCR, Subramania GS, Krishna S, Wasserman D (2019) Phonon-polaritons: enabling powerful capabilities for infrared photonics. *Nanophotonics* 8:2129
47. Forst M, Mankowsky R, Cavalleri A (2015) Mode-selective control of the crystal lattice. *Acc Chem Res* 48:380
48. Maier TA, Graser S, Hirschfeld PJ, Scalapino DJ (2011) *d*-Wave pairing from spin fluctuations in the  $\text{K}_x\text{Fe}_{2-y}\text{Se}_2$  superconductors. *Phys Rev B* 83:100515
49. Fanfarillo L, Mansart J, Toulemonde P, Cercellier H, Le Fevre P, Bertran F, Valenzuela B, Benfatto L, Brouet V (2016) Orbital-dependent Fermi surface shrinking as a fingerprint of nematicity in **FeSe**. *Phys Rev B* 94:155138
50. Rhodes LC, Watson MD, Haghighirad AA, Evtushinsky DV, Eschrig M, Kim TK (2018) Scaling of the superconducting gap with orbital character in **FeSe**. *Phys Rev B* 98:180503
51. Held K, Nekrasov I, Keller G, Eyert V, Blümer N, McMahan A, Scalettar R, Pruschke T, Anisimov V, Vollhardt D (2006) Realistic investigations of correlated electron systems with **LDA + DMFT**. *Phys Status Solidi (b)* 243:2599
52. Fukui T, Hatsugai Y, Suzuki H (2005) Chern numbers in discretized Brillouin zone: efficient method of computing (spin) Hall conductances. *J Phys Soc Jpn* 74:1674
53. Li Z, Han Y, Qiao Z (2022) Chern number tunable quantum anomalous Hall effect in monolayer transitional metal oxides via manipulating magnetization orientation. *Phys Rev Lett* 129:036801
54. Garanin DA (1997) Fokker-Planck and Landau-Lifshitz-Bloch equations for classical ferromagnets. *Phys Rev B* 55:3050
55. Gilbert TL (2004) A phenomenological theory of damping in ferromagnetic materials. *IEEE Trans Magn* 40:3443
56. Novikov I, Grabowski B, Kormann F, Shapeev A (2020) Machine-learning interatomic potentials reproduce vibrational and magnetic degrees of freedom. *arXiv preprint. arXiv:2012.12763*
57. Tranchida J, Plimpton S, Thibaudau P, Thompson A (2018) Massively parallel symplectic algorithm for coupled magnetic spin dynamics and molecular dynamics. *J Comput Phys* 372:406
58. Nikolov S, Wood MA, Cangi A, Maillet J-B, Marinica M-C, Thompson AP, Desjarlais MP, Tranchida J (2021) Data-driven magneto-elastic predictions with scalable classical spin-lattice dynamics. *npj Comput Mater* 7:153
59. Eckhoff M, Behler J (2021) High-dimensional neural network potentials for magnetic systems using spin-dependent atom-centered symmetry functions. *npj Comput Mater* 7:1
60. Yu H, Xu C, Li X, Lou F, Bellaïche L, Hu Z, Gong X, Xiang H (2022) Complex spin Hamiltonian represented by an artificial neural network. *Phys Rev B* 105:174422
61. Kresse G, Hafner J (1994) Ab initio molecular-dynamics simulation of the liquid-metal–amorphous-semiconductor transition in germanium. *Phys Rev B* 49:14251
62. Kresse G, Furthmüller J (1996) Efficiency of ab-initio total energy calculations for metals and semiconductors using a plane-wave basis set. *Comput Mater Sci* 6:15
63. Kresse G, Furthmüller J (1996) Efficient iterative schemes for ab initio total-energy calculations using a plane-wave basis set. *Phys Rev B* 54:11169
64. Kim H-J (2018) **VASPBerry**
65. Gordon E, Mkhitarian V, Zhao H, Lee Y, Ke L (2021) Magnetic interactions and spin excitations in van der Waals ferromagnet. *J Phys D, Appl Phys* 54:464001

## Publisher's Note

Springer Nature remains neutral with regard to jurisdictional claims in published maps and institutional affiliations.